J|A|C|S
A R T I C L E S

The Role of Electrostatics in Siderophore Recognition by the Immunoprotein Siderocalin[1]

Trisha M. Hoette,[†] Rebecca J. Abergel,[†] Jide Xu,[†] Roland K. Strong,[‡] and Kenneth N. Raymond*,[†]

Department of Chemistry, University of California, Berkeley, California 94720-1460, and Division of Basic Sciences, Fred Hutchinson Cancer Research Center, Seattle, Washington 98109

Received September 19, 2008; E-mail: raymond@socrates.berkeley.edu

Abstract: Iron is required for virulence of most bacterial pathogens, many of which rely on siderophores, small-molecule chelators, to scavenge iron in mammalian hosts. As an immune response, the human protein Siderocalin binds both apo and ferric siderophores in order to intercept delivery of iron to the bacterium, impeding virulence. The introduction of steric clashes into the siderophore structure is an important mechanism of evading sequestration. However, in the absence of steric incompatibilities, electrostatic interactions determine siderophore strength of binding by Siderocalin. By using a series of isosteric enterobactin analogues, the contribution of electrostatic interactions, including both charge−charge and cation−π, to the recognition of 2,3-catecholate siderophores has been deconvoluted. The analogues used in the study incorporate a systematic combination of 2,3-catecholamide (CAM) and *N*-hydroxypyridinonate (1,2-HOPO) binding units on a tris(2-aminoethyl)amine (tren) backbone, [tren(CAM)$_m$(1,2-HOPO)$_n$, where $m = 0$, 1, 2, or 3 and $n = 3 - m$]. The shape complementarity of the synthetic analogue series was determined through small-molecule crystallography, and the binding interactions were investigated through a fluorescence-based binding assay. These results were modeled and correlated through *ab initio* calculations of the electrostatic properties of the binding units. Although all the analogues are accommodated in the binding pocket of Siderocalin, the ferric complexes incorporating decreasing numbers of CAM units are bound with decreasing affinities ($K_d = >600$, 43, 0.8, and 0.3 nM for $m = 0-3$). These results elucidate the role of electrostatics in the mechanism of siderophore recognition by Siderocalin.

Introduction

Iron has a range of biologically relevant oxidation states, including Fe(II), Fe(III), and Fe(IV), and is therefore a platform for electron transfer, redox chemistry, and oxygen transport in living systems.[2] However, the availability of ferric ion is limited by its insolubility in aqueous, pH-neutral environments,[3] and the presence of ferrous ion poses the risk of the production of destructive oxygen radicals.[4] In response to these environmental pressures for tight regulation, both mammals and microorganisms have developed efficient and competitive systems to acquire, transport, and store iron.[3,5,6]

Of the 3−4 g of iron in the average human body, approximately 2.5 g participates in oxygen transport in hemoglobin, another 0.4 g is engaged in other cellular functions, and the small remaining portion of iron is bound by transport and storage proteins such as extracellular transferrins and intracellular ferritin.[7,8] With nearly all the iron confined to such proteins, the concentration of "free" extracellular iron is estimated at 10^{-24} M.[9] This iron containment strategy serves multiple physiological functions: first, to solubilize ferric ions which would otherwise be unavailable in a biological environment; second, to prevent ferrous ions from participating in unregulated production of reactive oxygen species (ROS) via the Fenton reaction; and finally, to act as a first line of defense against microbial infection by withholding iron.

Like mammals, microorganisms have developed effective systems to secure their iron supply. Many bacteria synthesize and secrete low-molecular-weight, highly iron-selective chelators called siderophores to collect iron from the extracellular environment.[8] There are hundreds of known siderophore structures with a variety of denticities, chelating units, and backbone scaffolds (Figure 1). Usually bacteria synthesize more than one type of siderophore (often a catecholate and a hydroxamate or citrate) by taking advantage of this modular

---

[†] University of California, Berkeley.

[‡] Fred Hutchinson Cancer Research Center.

(1) Paper #84 in the series Coordination Chemistry of Microbial Iron Transport. For previous paper, see: Abergel, R. J.; Clifton, M. C.; Pizarro, J. C.; Warner, J. A.; Shuh, D. K.; Strong, R. K.; Raymond, K. N. *J. Am. Chem. Soc.* **2008**, *130*, 11524–11534.

(2) *Iron Metabolism—Inorganic Biochemistry and Regulatory Metabolism*; Ferreira, G. C., Moura, J. J. C., Franco, R., Eds.; Wiley-VCH: Weinheim, 1999.

(3) Raymond, K. N.; Dertz, E. A. In *Iron Transport in Bacteria*; Crosa, J. H., Mey, A. R., Payne, S. M., Eds.; ASM Press: Washington, DC, 2004; pp 3–17.

(4) Pierre, J. L.; Fontecave, M.; Crichton, R. R. *Biometals* **2002**, *15*, 341–346.

(5) Hentze, M. W.; Muckenthaler, M. U.; Andrews, N. C. *Cell* **2004**, *117*, 285–297.

(6) Kontoghiorghes, G. J.; Weinberg, E. D. *Blood Rev.* **1995**, *9*, 33–45.

(7) Gordeuk, V. R.; Bacon, B. R.; Brittenham, G. M. *Annu. Rev. Nutr.* **1987**, *7*, 485–508.

(8) *Molecular and Cellular Iron Transport*; Templeton, D. M., Ed.; Marcel Dekker, Inc.: New York, 2002.

(9) Raymond, K. N.; Dertz, E. A.; Kim, S. S. *Proc. Natl. Acad. Sci. U.S.A.* **2003**, *100*, 3584–3588.
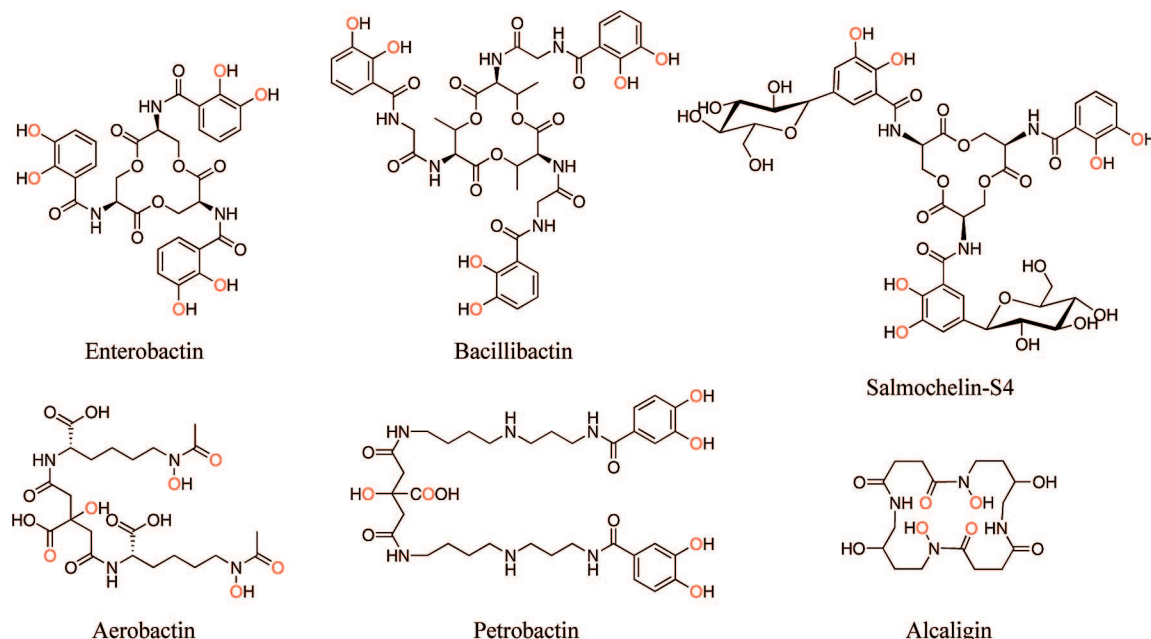

10.1021/ja8074665 CCC: $40.75

Figure 1. Selected siderophore structures, illustrating a variety of backbones and chelating moieties. Iron-binding atoms are shown in red. High-affinity, archetypal siderophores enterobactin and bacillibactin, from Gram-negative and Gram-positive bacteria, respectively, are sequestered by the immune system protein Siderocalin (Scn), while aerobactin (*Escherichia coli*), salmochelin-S4 (*Salmonella enterica*), petrobactin (*Bacillus anthracis*), and alcaligin (*Bordetella pertussis*) are not bound by Scn and confer virulence in the mammalian host.
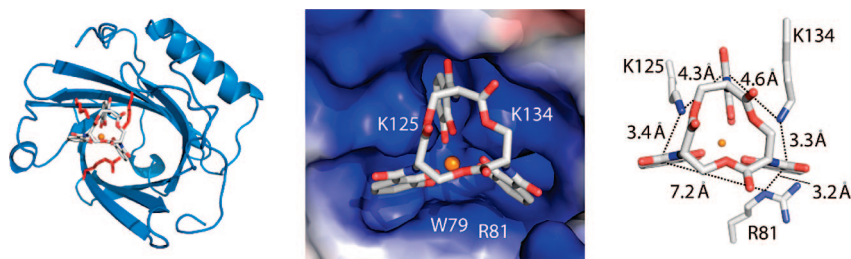

Figure 2. Enterobactin bound within the β-barrel of Scn (left). A space-filling, close-up view of the calyx showing positively charged residues in blue that shape the binding pocket (center). Cationic residues K125, K134, and R81 create a cyclically permuted cation−π interaction with enterobactin (right).

ligand assembly. In addition, most microorganisms are able to utilize xenosiderophores, expressing receptors for siderophores that the microbe does not itself produce.[10,11] The use of divergent, multi-siderophore systems by successful pathogens has proven to be an advantage against a number of environmental pressures, including the bacteriostatic action of the immune system in a mammalian host.

While containment of iron in a mammalian host is important as a preliminary protection against infection, many pathogens can overcome this limitation by producing siderophores, such as enterobactin and bacillibactin, that have a strong kinetic and thermodynamic advantage for removal of iron from transferrin.[12] In response to this action, the mammalian innate immune system produces Siderocalin (Scn, see Figure 2, also known as lipocalin 2, NGAL, uterocalin, and 24p3), a 20 kDa lipocalin that binds both ferric and apo siderophores, thereby preventing iron delivery.[13−16] The calyx (or binding site) of Scn is shallow and

lined with positive residues (K125, K134, and R81) that promote the binding of a number of different siderophores, including enterobactin and bacillibactin, which have the highest known affinities for iron. The recognition and the sub-nanomolar dissociation constant for the Scn/ferric enterobactin interaction are mediated by electrostatic bonds (including both Coulombic and cation−π) in the absence of good shape complementarity, atypical for tight protein/small-molecule binding. Nonetheless, recent work has shown that the most successful (and deadly) pathogens evade the host immune system by utilizing siderophores that are not recognized by Scn.

There are several examples in the literature that describe the substrate shape limitations of the Scn calyx. Successful pathogens such as *Bacillus anthracis* and *Salmonella enterica* use these shape constraints to their advantage by producing the "stealth siderophores", salmochelin[17,18] and petrobactin,[15] (Figure 1), which are not recognized because of gross steric incompatibilities with the rigid calyx. Hydroxamate-based

(10) Brickman, T. J.; Anderson, M. T.; Armstrong, S. K. *Biometals* **2007**, *20*, 303–322.
(11) Matzanke, B. F.; Bohnke, R.; Mollmann, U.; Reissbrodt, R.; Schunemann, V.; Trautwein, A. X. *Biometals* **1997**, *10*, 193–203.
(12) Carrano, C. J.; Raymond, K. N. *J. Am. Chem. Soc.* **1979**, *101*, 5401–5404.
(13) Flo, T. H.; Smith, K. D.; Sato, S.; Rodriguez, D. J.; Holmes, M. A.; Strong, R. K.; Akira, S.; Aderem, A. *Nature* **2004**, *432*, 917–921.
(14) Goetz, D. H.; Holmes, M. A.; Borregaard, N.; Bluhm, M. E.; Raymond, K. N.; Strong, R. K. *Mol. Cell* **2002**, *10*, 1033–1043.
(15) Abergel, R. J.; Wilson, M. K.; Arceneaux, J. E. L.; Hoette, T. M.; Strong, R. K.; Byers, B. R.; Raymond, K. N. *Proc. Natl. Acad. Sci. U.S.A.* **2006**, *103*, 18499–18503.
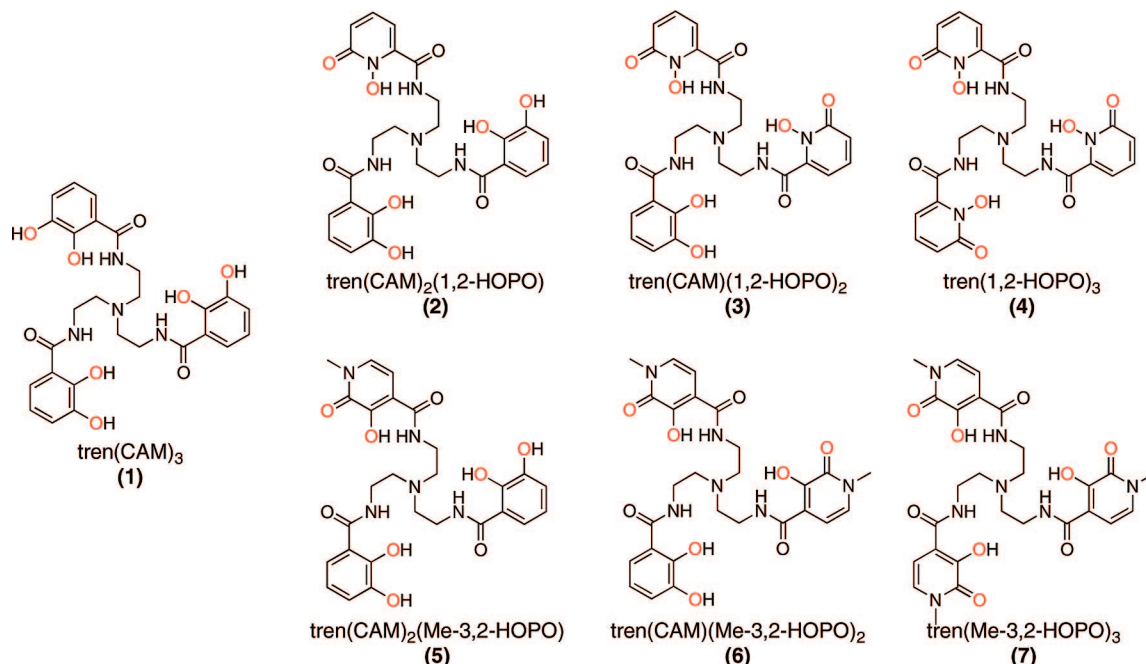(16) Holmes, M. A.; Paulsene, W.; Xu, J.; Ratledge, C.; Strong, R. K. *Structure* **2005**, *13*, 29–41.

Figure 3. Isosteric enterobactin analogues (**1**−**4**) and larger Me-3,2-HOPO analogues (**5**−**7**) used to study the influence of the electrostatic recognition of siderophores by Scn. The bidentate CAM and 1,2-HOPO groups have the same steric profile but pose different electrostatic interactions, whereas the Me-3,2-HOPO unit is similar electronically to the 1,2-HOPO unit but incorporates added steric bulk. Iron-binding atoms shown in red.

siderophores, which form neutral complexes, are another class of siderophores not bound by Scn.[14] Pathogens such as *Escherichia coli* and *Bordetella pertussis*, both of which can utilize enterobactin, instead rely on the hydroxamate siderophores, aerobactin[19] and alcaligin,[20] respectively (Figure 1), for virulence in a mammalian host.[21] While these systems similarly demonstrate that siderophore-mediated iron acquisition in pathogenic bacteria is closely associated with successful evasion of Scn, it raises the question: Do both steric and electronic features of siderophores contribute to Siderocalin recognition?

The work presented here aims to determine the relative contributions of the electrostatic components, both Coulombic and cation−π, to siderophore recognition through the use of an isosteric series of tris(2-aminoethyl)amine (tren)-based enterobactin analogues (tren(CAM)$_m$(1,2-HOPO)$_n$, **1**−**4**, Figure 3). The analogues incorporate a systematic combination of catecholamide (CAM) and 1,2-hydroxypyridinone (1,2-HOPO) metal-binding units. The isosteric nature of the ferric complexes was verified though small-molecule X-ray crystallography.[22] The sequestration by Scn of the apo, Fe^{III} and V^{IV} complex analogues was evaluated using fluorescence spectroscopy. A series of *ab initio* calculations were performed to study cation binding to the π face of the aromatic units. The Scn interactions with a larger analogue series (**5**−**7**) incorporating *N*-methyl-3,2-hy-
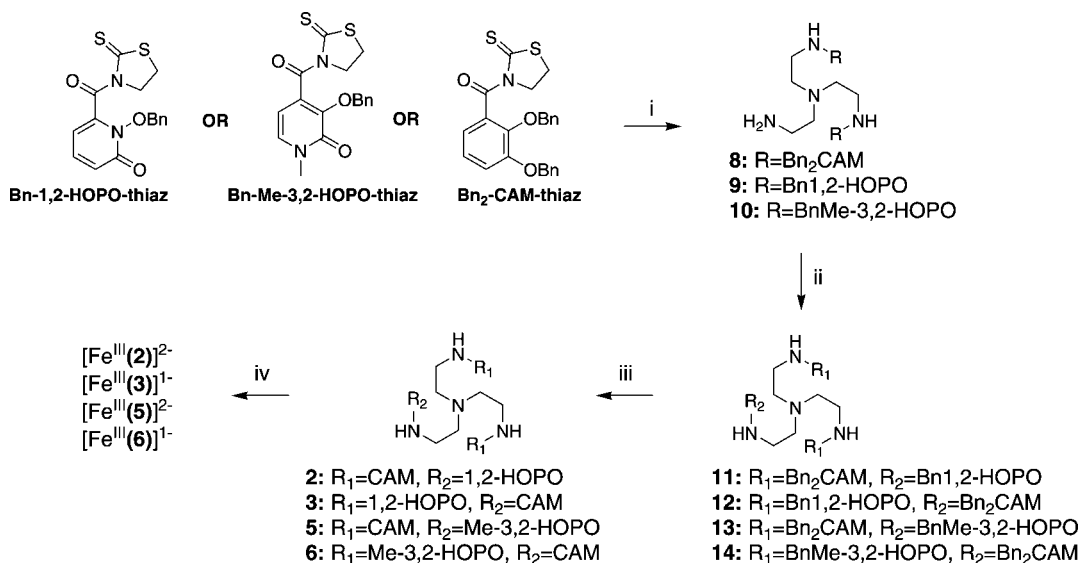
droxypyridinone binding units (Me-3,2-HOPO, Figure 3) were inspected as a parallel control for the isosteric 1,2-HOPO series. These studies demonstrate the importance of cation−π interactions to recognition, which, in concert with steric constraints imposed by the relatively rigid calyx, enables Scn to target unmodified catecholate siderophores but restricts binding of modified, virulence-associated "stealth" siderophores.

Results

Ligand and Metal Complex Synthesis. We have previously shown that ferric tren(CAM)$_3$, a well-studied synthetic analogue of enterobactin, binds to Scn with an affinity comparable to that of the ferric complex of the natural siderophore.[18] This and other studies indicated that the backbone is not an important part of recognition by Scn.[18] Syntheses of tren(CAM)$_3$,[23] tren(1,2-HOPO)$_3$,[24] and tren(Me-3,2-HOPO)$_3$[25] have been reported previously. The synthesis of the mixed binding unit analogues (Scheme 1) is based on methods previously described in the literature for multiple substitution of tren.[18,26] Slow addition of a stoichiometric (2:1) amount of thiazolide-activated benzyl-protected CAM, 1,2-HOPO, or Me-3,2-HOPO to the commercially available tren scaffold afforded the bis-substituted tren intermediate (**8**−**10**). A third binding unit was subsequently coupled, yielding the benzyl-protected ligands (**11**−**14**). The ligands were deprotected using acidic conditions (1:1 HCl: HOAc) and recrystallized from methanol and diethyl ether to afford the HCl salt of the ligands (**2**, **3** and **5**, **6**) in good yields. The iron complexes of all ligands were either prepared *in situ* (for fluorescence studies) or isolated (for crystallization). One

(17) Fischbach, M. A.; Lin, H. N.; Zhou, L.; Yu, Y.; Abergel, R. J.; Liu, D. R.; Raymond, K. N.; Wanner, B. L.; Strong, R. K.; Walsh, C. T.; Aderem, A.; Smith, K. D. *Proc. Natl. Acad. Sci. U.S.A.* **2006**, *103*, 16502−16507.

(18) Abergel, R. J.; Moore, E. G.; Strong, R. K.; Raymond, K. N. *J. Am. Chem. Soc.* **2006**, *128*, 10998−10999.

(19) Wooldridge, K. G.; Williams, P. H. *FEMS Microbiol. Rev.* **1993**, *12*, 325−348.

(20) Brickman, T. J.; Armstrong, S. K. *Infect. Immun.* **2007**, *75*, 5305−5312.

(21) Williams, P. H.; Warner, P. J. *Infect. Immun.* **1980**, *29*, 411−416.

(22) Macrae, C. F.; Edgington, P. R.; McCabe, P.; Pidcock, E.; Shields, G. P.; Taylor, R.; Towler, M.; van de Streek, J. *J. Appl. Crystallogr.* **2006**, *39*, 453−457.

(23) Rodgers, S. J.; Lee, C. W.; Ng, C. Y.; Raymond, K. N. *Inorg. Chem.* **1987**, *26*, 1622−1625.

(24) Xu, J.; Churchill, D. G.; Botta, M.; Raymond, K. N. *Inorg. Chem.* **2004**, *43*, 5492−5494.

(25) Xu, J.; O'Sullivan, B.; Raymond, K. N. *Inorg. Chem.* **2002**, *41*, 6731−6742.

(26) Cohen, S. M.; Raymond, K. N. *Inorg. Chem.* **2000**, *39*, 3624−3631.

Scheme 1. Synthesis of Tren-Based Enterobactin Analogues with Mixed Binding Units[a]

8: R=Bn$_2$CAM
9: R=Bn1,2-HOPO
10: R=BnMe-3,2-HOPO

[Fe^{III}(2)]$^{2-}$
[Fe^{III}(3)]$^{1-}$
[Fe^{III}(5)]$^{2-}$
[Fe^{III}(6)]$^{1-}$

2: R$_1$=CAM, R$_2$=1,2-HOPO
3: R$_1$=1,2-HOPO, R$_2$=CAM
5: R$_1$=CAM, R$_2$=Me-3,2-HOPO
6: R$_1$=Me-3,2-HOPO, R$_2$=CAM

11: R$_1$=Bn$_2$CAM, R$_2$=Bn1,2-HOPO
12: R$_1$=Bn1,2-HOPO, R$_2$=Bn$_2$CAM
13: R$_1$=Bn$_2$CAM, R$_2$=BnMe-3,2-HOPO
14: R$_1$=BnMe-3,2-HOPO, R$_2$=Bn$_2$CAM

[a] Reagents and conditions: (i) 0.5 equiv of tris(2-aminoethyl)amine, CH$_2$Cl$_2$; (ii) 1 equiv of Bn-1,2-HOPO-thiaz, Bn-Me-3,2-HOPO-thiaz, or Bn$_2$CAM-thiaz, CH$_2$Cl$_2$; (iii) 1:1 HCl:AcOH; (iv) Fe(acac)$_3$, KOH, MeOH, under N$_2$.
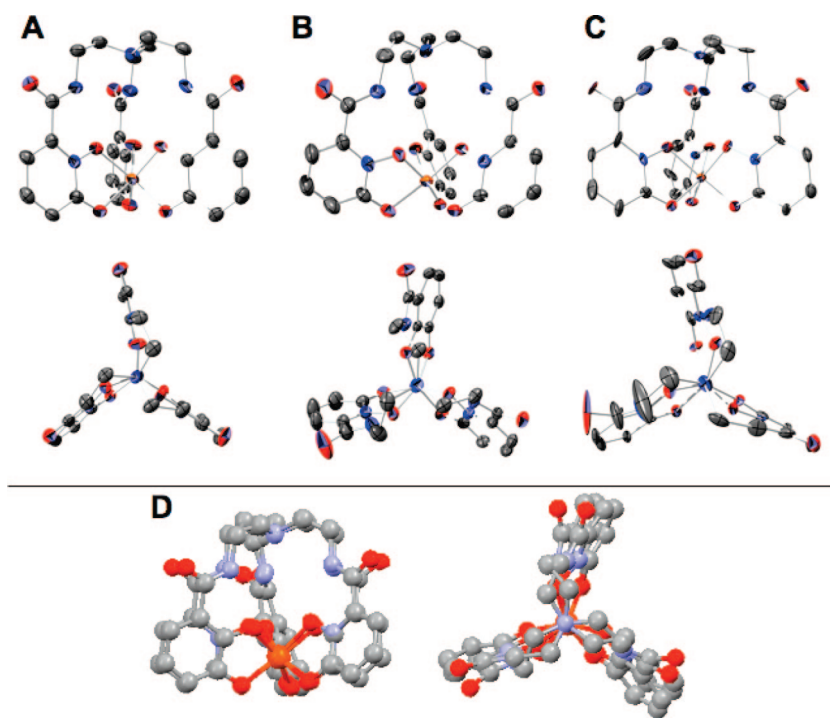

Figure 4. Structural diagrams (ORTEP), top and side views, of [Fe^{III}tren(CAM)$_2$(1,2-HOPO)]$^{2-}$ (A), [Fe^{III}tren(CAM)(1,2-HOPO)$_2$]$^-$ (B), and [Fe^{III}tren(1,2-HOPO)$_3$]^0 (C). Solvent molecules, counterions, and hydrogens are omitted for clarity (50% probability ellipsoids). Top and side views of MERCURY overlaid structures of [Fe^{III}tren(CAM)$_3$]$^{3-}$ and [Fe^{III}tren(1,2-HOPO)$_3$]^0 (D) with a room-mean-square deviation of 0.476 Å for the 34 atom pairs.

equivalent of Fe(acac)$_3$ was added to each of the ligands in methanol, followed by a stoichiometric amount of KOH to neutralize the HCl salt and deprotonate the ligand. In order to attain the complexes as solids, the metal complexes were recrystallized from diethyl ether. Potassium counterions were associated with the negatively charged complexes.

Solid-State Structures of [Fe^{III}(tren(CAM)$_m$(1,2-HOPO)$_n$)]$^{m-}$ and Structural Overlay of Isosteric Series. In order to demonstrate that the ligand series proposed would test only the electronic recognition of the ligands and their complexes and not their steric interaction, the X-ray structures of the ferric complexes were compared. While the structure of the trianionic

ferric tren(CAM)$_3$ complex has been previously described,[27] the solid-state characterization of the dianion, monoanion, and neutral ferric complexes is described here (Figure 4).

All three complexes, 2K$^+$[Fe^{III}(2)]$^{2-}$, K$^+$[Fe^{III}(3)]$^-$, and [Fe^{III}(4)]^0, crystallize in the monoclinic space group $P2_1/c$ (Table S1, Supporting Information), while 3K$^+$[Fe^{III}(1)]$^{3-}$ crystallizes in the cubic space group $P2_13$ (published structure). As described for [Fe^{III}(1)]$^{3-}$ and [V^{IV}(enterobactin)]$^{2-}$, the amide protons in these structures are directed inward and participate in a

(27) Stack, T. D. P.; Karpishin, T. B.; Raymond, K. N. *J. Am. Chem. Soc.* **1992**, *114*, 1512–1514.
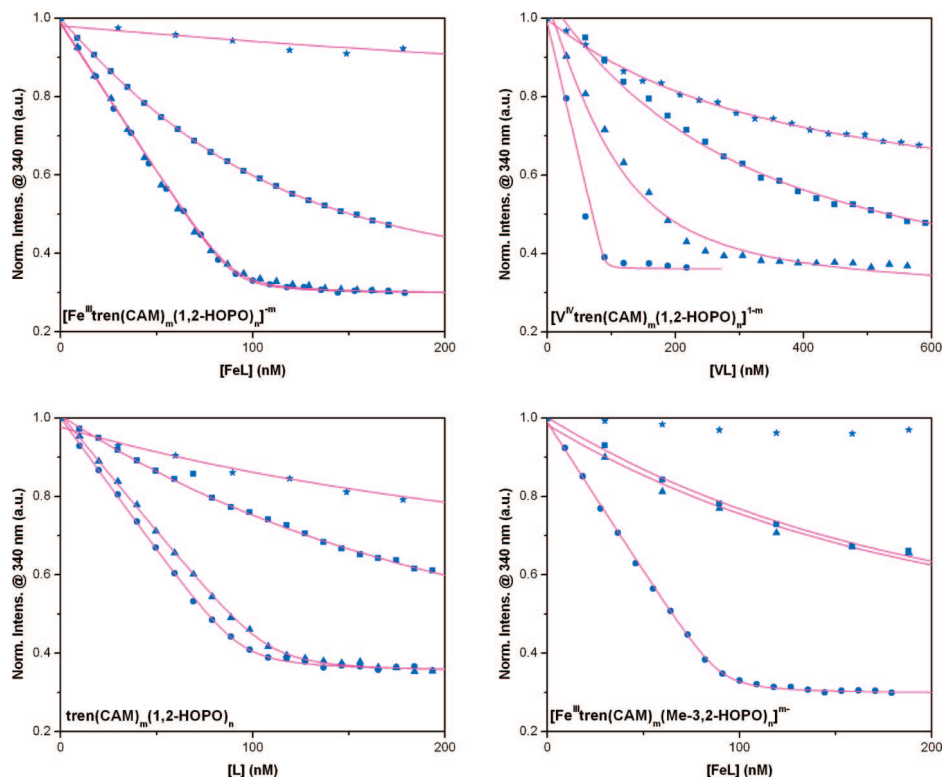
Figure 5. Fluorescence quenching titrations measuring the affinity of Scn for isosteric analogues **1−4** in the Fe[III] (top left), V[IV] (top right), and apo (bottom left) forms, as well binding curves with the Fe[III] complexes of mixed CAM ligands incorporating a bulkier Me-3,2-HOPO (bottom right). Experiments were performed with 100 nM Scn samples buffered at pH 7.4 with TBS. An excitation wavelength of 281 nm was used, and emission was monitored at 340 nm. The symbols represent the experimental fluorescence data (tren(CAM)$_m$(HOPO)$_n$: ●, $m = 3$, $n = 0$; ▲, $m = 2$, $n = 1$; ■, $m = 1$, $n = 2$; ★, $m = 0$, $n = 3$), and the calculated fits are shown as lines.

hydrogen-bonding network with the *o*-hydroxyls typical of these types of complexes.[27,28] The potassium counterions are either coordinated to an amide carbonyl or situated under the iron center interacting with the catecholate *m*-hydroxyls. There is no evidence of K⁺−π interactions in these small-molecule structures.

The tren-based ligands are achiral and therefore afford a racemic mixture of complexes (Δ and Λ). Two molecules of the same metal center chirality were used for the structural overlay. Since the backbone is not important to Scn recognition, only the binding units including the amides were used in the shape comparison. The ferric catecholamide units and the ferric hydroxypyridinone amide units of [Fe-tren(CAM)$_3$]$^{3-}$ and [Fe-tren(1,2-HOPO)$_3$]^0 were overlaid and distance minimized,[22] yielding a root-mean-square deviation for the 34 atom pairs of 0.476 Å (Figure 4). This shows that the complexes have virtually identical spatial arrangements, and Scn recognition should therefore differ only due to the electrostatic nature of the complexes.

Fluorescence Binding Assay. The affinities of Scn for the analogues were determined by a fluorescence-based binding assay as previously described.[14] A 100 nM solution of Scn was titrated with between 2 and 10 equiv of substrate, depending on the affinity. The binding curves were fit by nonlinear least-squares refinement and the resulting dissociation constants calculated.[29] Four sets of substrates were used in this study: Fe[III] and V[IV] complexes of the tren(CAM)$_m$(1,2-HOPO)$_n$ series were used for direct comparison of complex charge; apo ligands

were used to explore the recognition of the aromatic units; and ferric complexes of a series of ligands incorporating the structurally similar Me-3,2-HOPO unit (Figure 3) rather than the 1,2-HOPO unit were studied, combining both steric and electronic perturbations as a parallel control for the isosteric 1,2-HOPO series. Binding results are shown in Figure 5 and Table 1. Crystallographic analyses of complexes between Scn and the isosteric 1,2-HOPO series show that, in general, these compounds bind in the calyx in the same orientation as enterobactin (Clifton et al., manuscript in preparation), making them ideal compounds for isolating the relative effects of cation−π versus Coulombic bonds.

A decrease of affinity was observed within the ligand series for both the ferric and vanadium complexes with decreasing charge. In a comparison of a ferric complex to the vanadium complex with the same ligand, there is a decrease in affinity for every pair of substrates. In addition, the charge-matched complexes are bound with comparable K_d's for the pairs of complexes. The more highly charged complexes (3− and 2−) are recognized with fairly strong affinities with only slight charge effect. The complexes of lesser charge (1−, neutral, and 1+) experience a more dramatic decrease in recognition compared to larger anions, such that binding was barely detectable under the experimental conditions.

The apo ligands were also tested for Scn binding. The charges on the ligands were estimated from the previously determined protonation constants for tren(CAM)$_3$ and tren(1,2-HOPO)$_3$. Since the 1,2-HOPO unit is a relatively acidic binding unit (in

(28) Karpishin, T. B.; Dewey, T. M.; Raymond, K. N. *J. Am. Chem. Soc.* **1993**, *115*, 1842−1851.

(29) Kuzmic, P. *Anal. Biochem.* **1996**, *237*, 260−273.

Table 1. Scn Affinities for Tren-Based Analogues and Their Metal Complexes[a]

	K_d		
	Fe[III]	V[IV]	no metal
trenCAM₃	0.3 ± 0.1 nM[18]	1.3 ± 0.3 nM	1.2 ± 0.2 nM
trenCAM₂(1,2-HOPO)	0.8 ± 0.3 nM	40 ± 9 nM	1.4 ± 0.3 nM
trenCAM₂(Me-3,2-HOPO)	0.12 ± 0.01 μM	n.d.	n.d.
trenCAM(1,2-HOPO)₂	43 ± 2 nM	0.22 ± 0.07 μM	0.14 ± 0.01 μM
trenCAM(Me-3,2-HOPO)₂	0.15 ± 0.02 μM	n.d.	n.d.
tren(1,2-HOPO)₃	>0.6 μM	0.30 ± 0.03 μM	0.25 ± 0.03 μM
tren(Me-3,2-HOPO)₃	>0.6 μM	n.d.	n.d.

[a] Dissociation constants are reported in units of either nM or μM depending on the magnitude in order to maintain consistent significant figures. See Supporting Information (Figure S1) for a bar graph representation of Scn dissociation constants.
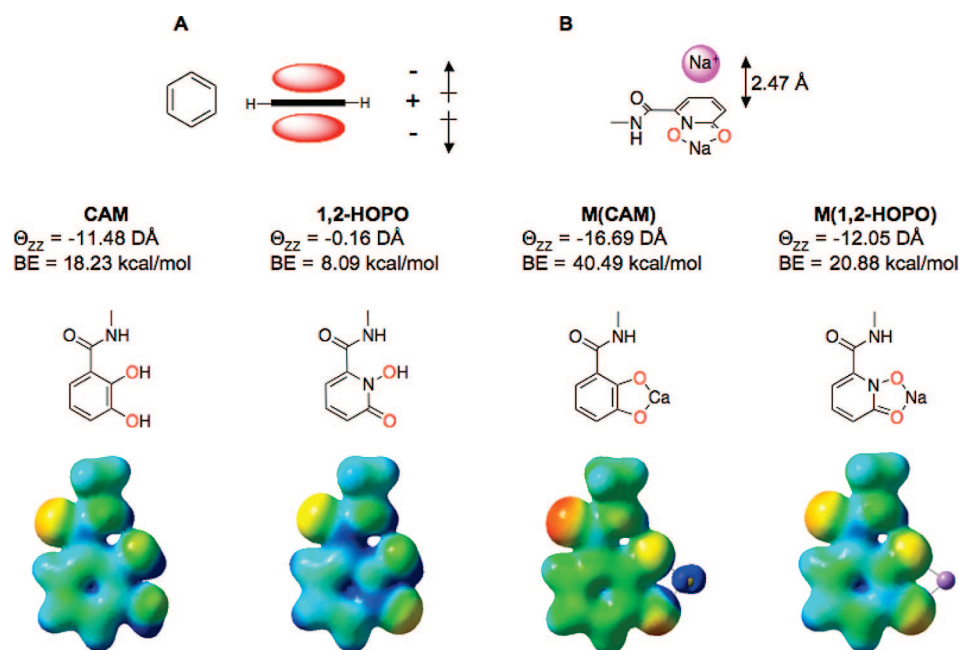

Figure 6. Schematic of the quadrupole moment of benzene with negative density above and below the ring represented in red (A). Representative input structure for calculations of cation−π interactions energies with the model aromatic units; as shown here, the cation (in pink) was fixed at 2.47 Å above the centroid of the M(1,2-HOPO) aromatic (B). Computational studies describe the electrostatic interactions of metal-binding units of siderophores with positive residues of the calyx. The bottom panel includes quadrupole moments (calculated at the level RHF/6-311G** of theory), cation−π interaction energies (calculated at MP2/6-311++G** the level of theory), molecular structures, and electrostatic potentials (with a range of −0.18 (red) to +0.18 kcal/mol (blue)) for the four model aromatic units used in this study.

tren(1,2-HOPO)₃, pK_{aHOPO} = 3.60, 4.32, 5.62[30]), the hydroxyl will be deprotonated in our experimental conditions (pH 7.4). For the more basic CAM unit (in tren(CAM)₃, pK_{aCAM} = 6.71, 8.61, 8.75, 11.3, 12.1, 12.9[23]), only one of the *meta* oxygens is deprotonated at pH 7.4; therefore, the overall ligand charge at physiological pH is 1−. The fluorescence binding data indicated that Scn affinity decreased with increasing 1,2-HOPO content, in that tren(CAM)₃ is recognized with sub-nanomolar affinity while tren(1,2-HOPO)₃ is bound in a micromolar affinity range.

Relative to the 1,2-HOPO series, the Me-3,2-HOPO analogue series provides a platform for comparison of the influence of shape versus charge. An additional methyl group functionalizes the N group on the binding unit, placing more steric demand on the bottom side of the binding unit. The addition of both one and two Me-3,2-HOPO units decreases the affinity 3 orders of magnitude compared to that of the parent *tris*-catecholate. The complex with three Me-3,2-HOPO units is not bound.

***Ab Initio* Calculations of Quadrupole Moments and Cation−π Interaction Energies.** Two sets of *ab initio* calculations were performed to examine the interactions of the π surfaces of a siderophore with cationic residues in the calyx of Scn. The methyl amide bidentate units of CAM and 1,2-HOPO were used as a simplified model (Figure 6). In order to mimic coordination to a metal center, the 1,2-HOPO and CAM units were coordinated to alkaline metal ions, sodium and calcium, respectively, to form the neutral metal complexes. The free ligand forms of the bidentate units were also studied. These four molecules were geometry optimized, and the quadrupole tensor components were determined at the RHF/6-311G** level of theory.[31]

Next, the cation interaction energies with the π surfaces of the four aromatic units were determined at the MP2/6-311++G** level of theory, and the basis set superposition error was corrected for with the counterpoise method.[31] A cation was placed above the centroid of the aromatic at 2.47 Å, as described

(30) Jocher, C. J.; Moore, E. G.; Xu, J.; Avedano, S.; Botta, M.; Aime, S.; Raymond, K. N. *Inorg. Chem.* **2007**, *46*, 9182–9191.

(31) Frisch, M. J.; et al. *Gaussian 03*, Revision C.02; Gaussian, Inc.: Wallingford, CT, 2004.

in the literature[32] (Figure 6B). In these calculations, a sodium ion was used as a non-polarizable model cation, as is common practice in these types of calculations.[32,33] Since these molecules have alternate binding sites for the cation (for example, the amide carbonyl), the geometry was fixed with the cation above the centroid of the previously optimized π system. In these calculations, a purely electrostatic model was employed and, therefore, did not account for the influence of polarizability in the cation–π system. Nonetheless, this model has proven suitable for comparison of cation–π interactions within an aromatic series.[32]

The anisotropy of the tensor components of the four molecules used in these calculations was calculated as $\Theta_{zz} = Q_{zz} - 0.5(Q_{xx} + Q_{yy})$. The quadrupole moments calculated for the neutral molecules were within the range of values reported for similarly functionalized aromatics.[33] Both CAM molecules were found to have more negative Θ_{zz} values than their 1,2-HOPO counterparts. In comparing the protonated molecules to the metal complexes, both CAM and 1,2-HOPO experienced a more negative Θ_{zz} upon metal binding (Figure 6). Calculated cation interaction energies with these metal-binding units confirmed that, as Θ_{zz} becomes more negative, the binding energy increases.

Discussion

Recognition by Coulombic Interactions. A comparison of the dissociation constants of the Fe^{III} complexes and the V^{IV} complexes provides direct evidence of the effect of substrate charge on recognition. Previous work has shown that the Scn recognition of $[V^{IV}(enterobactin)]^{2-}$ is slightly weaker than for $[Fe^{III}(enterobactin)]^{3-}$.[18] The present study expands on this result, demonstrating the generality of the charge effect on Scn recognition. Since there is a significant difference in binding between the neutral and monoanionic complexes compared to the dianionic and trianionic complexes, it appears that Scn favors at least dianionic substrates for strong recognition. In addition, Fe^{III} and V^{IV} complexes of the same charge (different ligands), for example $[Fe^{III}(tren(CAM)(1,2-HOPO)_2)]^-$ and $[V^{IV}(tren(CAM)_2(1,2-HOPO))]^-$, have the same binding affinity within experimental error.

The catecholate binding unit, when compared to the hydroxamate, has enhanced stability with iron that increases from the bidentate to tetradentate to hexadentate complexes. For example, while the tris-hydroxamate desferrioxamine B has a pM value of 26.6, the tris-catecholate enterobactin has a pM value of 35.3 (where pM = $-\log[Fe^{III}]$ at $[L] = 10 \ \mu\text{mol L}^{-1}$ and $[Fe^{III}] = 1 \ \mu\text{mol L}^{-1}$),[34] making it a far superior ligand for iron binding.[3] Catecholate complexes of ferric ion are highly anionic due to the dianionic bidentate unit.[35] Therefore, Scn impedes iron scavenging via catecholate siderophores by recognizing these anionic substrates through Coulombic electrostatic binding interactions.

Recognition by Cation–π Interactions. A cation–π interaction has a distance dependence of $1/r^n$, where $n < 2$, similar to the $1/r$ dependence in a Coulombic interaction.[36] However,

while a Coulombic attraction provides a strong interaction between two charged groups, the cation–π interaction creates a specific interaction dependent upon geometric constraints. The calculated quadrupole moments and cation–π interaction energies for the 2,3-catecholamide structures support the experimental observation that, in general, the CAM-containing ligands have stronger binding affinities with Scn than the 1,2-HOPO ligands. This becomes most apparent when comparing the binding trend for the apo ligands. While the tris-substituted 1,2-HOPO ligand, with an overall 3– charge, binds weakly to Scn, the tris-substituted CAM ligand has an overall 1– charge and is bound much more tightly. Thus, it appears that the cation–π interaction of the 2,3-catecholamide is more important to binding than the Coulombic attraction between the anionic substrate and the cationic calyx. The recognition of apo catecholate siderophores is biologically relevant, since it has previously been demonstrated that both apo bacillibactin and apo enterobactin are bound with high affinity by Scn.[15,18]

Overall Recognition Mechanism. This study has focused on the importance of the electronic character of a siderophore to Scn recognition, demonstrating that the electrostatic nature, including the quadrupole of aromatics and the overall charge of the substrate, is important to selectivity. Whereas previous studies have shown that large adducts also affect selectivity by introducing intolerable steric clashes, here we show that even the *N*-methyl substituent on the Me-3,2-HOPO unit is not accommodated. It has been shown previously that neither the backbone nor the metal, nor the chirality at the metal center, is important for recognition by Scn.[15,18] The features of the metal-binding units seem to single-handedly influence whether Scn binds a substrate.

One of the most remarkable features of Scn is that it can bind a number of substrates of differing structures while maintaining an affinity comparable to that of cognate siderophore receptors, in order to act effectively as a bacteriostatic agent. The recognition mechanism relies on interactions between the protein and key substructures of the substrate rather than global recognition of the entire ligand. This recognition degeneracy may also enable the protein to participate in moonlighting functions. Scn has been implicated in several other physiological events unrelated to bacteremia, such as iron trafficking, tissue development, and apoptosis.[37–39] Recognition mechanisms that broaden the specificity of Scn–ligand interactions may, therefore, extend to as-yet uncharacterized endogenous ligands that mediate pleiotropic functions of Scn.

Conclusion

Scn has an affinity for ferric enterobactin similar to that of the siderophore's bacterial membrane receptor FepA, making it an effective competitor as part of an immune response against bacterial iron theft. Scn also binds ferric bacillibactin with equal affinity. Bacillibactin and enterobactin are the archetypal siderophores of Gram-positive and Gram-negative bacteria, respectively. Both are tripodal 2,3-catecholates based on trilactone backbones, which provides these compounds unrivaled affinities for ferric ion. But, because of Scn, neither siderophore contributes to virulence.

(32) Mecozzi, S.; West, A. P.; Dougherty, D. A. *J. Am. Chem. Soc.* **1996**, *118*, 2307–2308.
(33) Tran, D.; Beg, S.; Clements, A.; Lewis, M. *Chem. Phys. Lett.* **2006**, *425*, 347–352.
(34) Pecoraro, V. L.; Weitl, F. L.; Raymond, K. N. *J. Am. Chem. Soc.* **1981**, *103*, 5133–5140.
(35) Karpishin, T. B.; Gebhard, M. S.; Solomon, E. I.; Raymond, K. N. *J. Am. Chem. Soc.* **1991**, *113*, 2977–2984.

(36) Dougherty, D. A. *Science* **1996**, *271*, 163–168.
(37) Devireddy, L. R.; Gazin, C.; Zhu, X. C.; Green, M. R. *Cell* **2005**, *123*, 1293–1305.
(38) Kaplan, J. *Cell* **2002**, *111*, 603–606.
(39) Schmidt-Ott, K. M.; Mori, K.; Li, J. Y.; Kalandadze, A.; Cohen, D. J.; Devarajan, P.; Barasch, J. *J. Am. Soc. Nephrol.* **2007**, *18*, 407–413.

On the basis of this study, we conclude that hydroxamates do not bind to Scn, in part due to the formation of neutral ferric complexes and the lack of aromatic binding units, the hallmark structural unit recognized by Scn. Hydroxamates, while having a lower affinity for iron compared to catecholate siderophores, may be the workhorse siderophores for many organisms because they are not impeded by Scn. Many microorganisms rely on a dual siderophore system for iron acquisition, often including a catecholate and a hydroxamate. While this strategy offers several advantages, including the ability to adapt to varying degrees of environmental stress, one reason to employ a hydroxamate siderophore in a mammalian host is to ensure virulence in the presence of the bacteriostatic action of the immune system.

Experimental Section

General. Unless otherwise noted, starting materials were obtained from commercial suppliers and were used without further purification. Flash silica gel chromatography was performed using Merck silica gel (40-7 mesh). Microanalyses were performed by the Microanalytical Services Laboratory, College of Chemistry, University of California, Berkeley. Mass spectra were recorded at the Mass Spectrometry Laboratory, College of Chemistry, University of California, Berkeley. Melting points were taken on a Büchi melting apparatus and are uncorrected. All ^{1}H NMR and ^{13}C NMR spectra were recorded on AV-300 or AVB-400 Bruker FT spectrometers unless otherwise noted. Tren(CAM)$_3$ (**1**),[23] tren(1,2-HOPO)$_3$ (**4**),[24] tren(Me-3,2-HOPO)$_3$ (**7**),[25] Bn$_2$-2,3-CAM-thiaz,[26] Bn-1,2-HOPO-thiaz,[24] Bn-Me-3,2-HOPO-thiaz,[40] and [Fe^{III}tren-(CAM)$_3$]$^{3-}$ [27] were prepared according to published procedures.

Syntheses. The syntheses of all of the mixed ligands followed the same process, as illustrated in Scheme 1. The synthetic procedure of tren(CAM)$_2$(1,2-HOPO) is fully described, as well as the synthesis of the iron complex [Fe^{III}tren(CAM)$_2$(1,2-HOPO)]$^{2-}$, as representative examples for the syntheses all of the other intermediates, ligands, and iron complexes. Complete characterizations for all new compounds are included.

Bn-tren(CAM)$_2$(1,2-HOPO) (11). 2,3-Benzyloxybenzoylmercaptothiazoline (Bn$_2$-2,3-CAM-thiaz) (1.334 g, 3.062 mmol, 2 equiv) was dissolved in chloroform (150 mL) and added dropwise via capillary over 4 days to tris(2-aminoethyl)amine (0.229 mL, 1.531 mmol, 1 equiv) in dichloromethane (50 mL). The resulting mixture was evaporated to dryness, and the presence of the bis-substituted intermediate **8** was confirmed by proton NMR, at which point the crude material was carried into the next step without further purification. ^{1}H NMR (300 MHz, CDCl$_3$): δ 7.92 (t-br, 2H), 7.59−7.09 (m, 22H), 7.07 (d, J = 8.1 Hz, 4H), 5.10 (s, 4H, CH_2), 5.02 (s, 4H, CH_2), 3.18 (q, J = 6.3 Hz, 4H, CH_2), 2.45 (t, J = 6 Hz, 2H, CH_2), 2.35 (t, J = 6.6 Hz, 6H, CH_2), 1.86 (s, 2H, NH_2) ppm.

The bis-substituted intermediate **8** (0.990 g, 1.271 mmol) was dissolved in CH$_2$Cl$_2$ and added to *N*-benzyloxypyridin-2-one-6-mercaptothiazoline (Bn-1,2-HOPO-thiaz) (0.440 g, 1.271 mmol, 1 equiv) in CH$_2$Cl$_2$. The reaction mixture was stirred until the starting material was consumed (the solution went from yellow to clear). The reaction mixture was extracted with 1 M NaOH three times, dried over Na$_2$SO$_4$, and condensed. The resulting residue was applied to a silica column, and product was eluted with 2:98 CH$_3$OH:CH$_2$Cl$_2$. The fractions containing the protected ligand **11** were combined, and the solvent was evaporated to obtain the product as clear oil. Yield: 62%. ^{1}H NMR (300 MHz, CDCl$_3$): δ 7.82 (t-br, 2H), 7.65 (t-br, 1H), 7.32−6.98 (m, 32H), 6.53 (d, J = 7.8 Hz, 1H), 6.11 (d, J = 5.1 Hz, 1H), 5.33 (s, 2H), 5.09 (s, 4H), 4.99 (s, 4H), 3.12 (m, 6H), 2.48 (t-br, 2H), 2.27 (t, J = 6.3 Hz, 4H) ppm. ^{13}C NMR (75 MHz, CDCl$_3$): δ 165.92, 161.26, 158.99, 152.04, 146.94, 143.92, 138.29, 136.93, 136.80, 134.42, 130.56,

(40) Xu, J.; Franklin, S. J.; Whisenhunt, D. W.; Raymond, K. N. *J. Am. Chem. Soc.* **1995**, *117*, 7245–7246.

129.43, 129.12, 129.08, 129.06, 128.83, 128.67, 128.14, 127.70, 124.79, 123.72, 123.17, 117.11, 105.29, 53.99, 53.69, 52.19, 38.15, 37.62 ppm. (+)FABMS (MH$^+$): calcd, 1006; obsd 1006.

Tren(CAM)$_2$(1,2-HOPO) (2). Bn-tren(CAM)$_2$(1,2-HOPO) (**11**) (2.580 g, 2.565 mmol) was dissolved in 1:1 HCl:CH$_3$COOH. The mixture was stirred overnight and the solution evaporated to dryness. The product was recrystallized by dissolving the crude residue in minimum amount of CH$_3$OH and dripped slowly into 50 mL of stirring ether in a polypropylene tube. The slurry was then centrifuged and the ether decanted to obtain the deprotected ligand **2** as a white solid. Yield: 68%. Mp: 152−155 °C. ^{1}H NMR (300 MHz, DMSO): δ 9.12 (m, 3H), 7.39 (dd, J = 6.9, 2.1 Hz, 1H), 7.33 (d, J = 7.2 Hz, 2H), 6.94 (d, J = 6.9 Hz, 2H), 6.70 (t, J = 7.8 Hz, 2H), 6.59 (dd, J = 9, 1.5 Hz, 1H), 6.40 (dd, J = 6.9, 1.5 Hz, 1H), 3.73 (m, 6H), 3.37 (m, 6H) ppm. ^{13}C NMR (75 MHz, DMSO-d_6): δ 170.13, 157.48, 149.31, 146.20, 137.18, 119.09, 118.16, 117.71, 115.07, 104.38, 51.51, 33.85 ppm. (+)FABMS (MH$^+$): calcd, 556; obsd, 556. Anal. Calcd (found) for C$_{26}$H$_{29}$N$_5$O$_9$·HCl·H$_2$O: C, 49.64 (49.86); H, 5.13 (5.44); N, 11.13 (10.84).

[Fe^{III}tren(CAM)$_2$(1,2-HOPO)]$^{2-}$ ([Fe^{III}(2)]$^{2-}$). Tren(CAM)$_2$(1,2-HOPO) (**2**) (24.3 mg, 0.041 mmol) was dissolved in methanol (10 mL) and degassed. Fe(acac)$_3$ (14.5 mg, 1 equiv) was dissolved in methanol (5 mL) and added to the ligand solution, followed by 3 equiv of KOH (0.095 M in MeOH). The solution was degassed and stirred under N$_2$ overnight. The iron complex solution was condensed (not to dryness) and precipitated with ether. The purple solid was filtered. Yield: 20.1 mg (81 %). Mp: 300 °C. (−)ESMS (M − H$^-$): calcd, 607; obsd, 607. Anal. Calcd (found) for [C$_{26}$H$_{24}$N$_5$O$_9$Fe]$^{2-}$2K$^+$·3H$_2$O: C, 42.29 (42.08); H, 4.10 (4.19); N, 9.48 (9.12).

Tren(CAM)(1,2-HOPO)$_2$ (3). The bis-substituted intermediate **9** was confirmed by ^{1}H NMR (300 MHz, CDCl$_3$): δ 7.42 (t-br, 2H), 7.24 (m-br, 2H), 7.12 (t, J = 6.9 Hz, 2H), 6.42 (d, J = 9 Hz, 2H), 6.10 (d, J = 6.6 Hz 2H, ArH), 5.21 (s, 4H, CH_2), 3.15 (m, 6H), 2.29 (m, 4H), 2.04 (m, 2H) ppm.

Yield of **12** (clear oil): 59%. ^{1}H NMR (300 MHz, CDCl$_3$): δ 8.08 (t, J = 6.3 Hz, 1H), 7.47−6.93 (m, 24H), 6.85 (t, J = 8.1 Hz, 2H), 6.58 (d, J = 9.3 Hz, 2H), 6.08 (d, J = 6.6 Hz, 2H), 5.30 (s, 4H), 5.13 (s, 2H), 4.90 (s, 2H), 3.14 (m, 4H), 3.05 (m, 2H), 2.42 (m, 4H), 2.15 (m, 2H) ppm; ^{13}C NMR (75 MHz, DMSO-d_6): δ 170.10, 160.69, 157.49, 146.22, 141.46, 137.22, 130.56, 129.43, 129.12, 129.08, 129.06, 128.83, 128.67, 128.14, 127.70, 120.05, 118.15, 117.70, 115.03, 104.38, 51.07, 33.89 ppm. (+)FABMS (MLi$^+$): calcd, 923; obsd, 923.

Yield of **3** (white powder), 67%. Mp: 161−163 °C. ^{1}H NMR (300 MHz, DMSO): δ 9.15 (m, 3H), 7.40 (m, 3H), 6.95 (d, J = 6.9 Hz, 1H), 6.70 (t, J = 7.8 Hz, 1H), 6.60 (dd, J = 7.5, 1.8 Hz, 2H), 6.43 (dd, J = 5.4, 1.5 Hz, 2H), 3.70 (m, 6H), 3.45 (m, 6H) ppm. ^{13}C NMR (75 MHz, DMSO-d_6): δ 161.40, 158.19, 150.04, 146.92, 142.16, 137.92, 105.08, 51.70, 34.61 ppm. (+)FABMS (MH$^+$): calcd, 557; obsd, 557. Anal. Calcd (found) for C$_{25}$H$_{28}$N$_6$O$_9$·HCl·H$_2$O: C, 47.65 (47.83); H, 4.96 (5.16); N, 13.30 (12.85).

Yield of [Fe^{III}(**3**)]$^-$ (bluish purple solid): 70 %. Mp: >300 °C. (−)ESMS (M − H): calcd, 608; obsd, 608. Anal. Calcd (found) for [C$_{25}$H$_{24}$N$_6$O$_9$Fe]$^-$K$^+$·2H$_2$O·CH$_3$OH: C, 43.65 (43.49); H, 4.50 (4.19); N, 11.75 (11.35).

Tren(CAM)$_2$(Me-3,2-HOPO) (5). Yield of **13** (clear oil): 77%. ^{1}H NMR (300 MHz, CDCl$_3$): δ 7.84 (t-br, 2H), 7.79 (t-br, 1H), 7.64 (t, J = 4.8 Hz, 2H), 7.08−7.50 (m, 29H), 6.99 (d, J = 7.2 Hz, 1H), 6.64 (d, J = 7.2 Hz, 1H), 5.29 (s, 2H), 5.14 (s, 4H), 5.04 (s, 4H), 3.52 (s, 3H), 3.16 (q-br, J = 6 Hz), 3.10 (t, J = 4.0 Hz, 2H), 2.31 (s-br, 6H) ppm. ^{13}C NMR (300MHz, CDCl$_3$): δ 164.8, 162.9, 159.0, 151.3, 146.2, 145.7, 136.2, 136.0, 131.8, 130.5, 128.4, 128.2, 127.8, 127.3, 127.2, 123.9, 122.5, 116.3, 104.3, 75.8, 74.2, 70.7, 52.1, 51.7, 45.7, 37.2, 36.8 ppm. (+)FABMS: *m/z* 1020.5 (MH$^+$).

Yield of **5** (white powder): 73%. Mp: 115−118 °C. ^{1}H NMR (400 MHz, DMSO-d_6): δ 12.15 (s-br, 2H), 11.35 (s-br, 1H), 10.06

(s-br, 1H), 9.26 (s-br, 1H), 9.01 (t-br, 2H), 8.68 (t-br, 1H), 7.27 (d, $J = 7.6$ Hz, 2H), 7.14 (d, $J = 7.2$ Hz, 1H), 6.92 (d, $J = 7.6$ Hz, 2H), 6.68 (t, $J = 8.0$ Hz, 2H), 6.45 (d, $J = 7.2$ Hz, 1H), 3.72 (m-br, 6H), 3.46 (m 9H) ppm. ^{13}C NMR (400 MHz, DMSO-d_6): δ 172.0, 170.1, 166.1, 158.1, 149.4, 147.5, 146.2, 127.7, 119.1, 118.1, 117.7, 117.0, 115.0, 102.9, 51.6, 45.4, 36.9, 33.8, 21.1 ppm. (+)FABMS: m/z 570.5 (MH$^+$). Anal. Calcd (found) for $C_{27}H_{31}N_5O_9 \cdot 2H_2O$ (FW 605.59): C, 53.55 (53.28); H, 5.83 (5.95); N, 11.56 (11.21).

Yield of [Fe^{III}(**5**)]$^{2-}$ (reddish purple solid): 80%. Mp: >300 °C. (−)FABMS: m/z 621 [(HM)$^-$]. Anal. Calcd (found) for K$_2$[FeC$_{27}$H$_{26}$N$_5$O$_9$]·3H$_2$O (FW 752.61): C, 43.09 (42.78); H, 4.29 (4.12); N, 9.31 (9.01).

Tren(CAM)(Me-3,2-HOPO)$_2$ (6). Yield of **14** (clear oil): 65%. ^{1}H NMR (400 MHz, CDCl$_3$): δ 1.64 (s, 6H), 3.08 (s, br, 4H), 3.10 (s, br, 4H), 3.58 (s, br, 2H), 3.61 (s, br, 2H) 5.16 (s, 4H), 5.61 (s, 4H), 6.54 (d, $J = 7.2$ Hz, 2H), 7.06 (d, $J = 7.2$ Hz, 2H), 7.29−7.43 (m, 20H), 7.61 (d, $J = 8.4$ Hz, 1H), 7.82 (d, $J = 8.4$ Hz, 1H), 8.24 (m, br, 3H) ppm. (+)FABMS: m/z 946.0 (MH$^+$). Anal. Calcd (found) for $C_{55}H_{56}N_6O_9$: C, 69.90 (70.17); H, 5.97 (6.22); N, 8.89 (8.75).

Yield of **6** (off white solid): 88%. Mp: 103−105 °C. ^{1}H NMR (500 MHz, DMSO-d_6): δ 3.46 (br, 12H), 3.70 (s, br, 6H), 6.44 (d, $J = 7.0$ Hz, 2H), 6.68 (t, $J = 8.0$ Hz, 1H), 6.93 (d, $J = 7.5$ Hz, 1H), 7.14 (d, $J = 7$ Hz, 2H), 7.26 (d, $J = 7.5$ Hz, 1H), 8.67 (br, 2H), 8.98 (br, 1H), 9.91 (br, 1H), 12.13 (br, 1H) ppm. ^{13}C NMR (500 MHz, DMSO-d_6): δ 34.03, 36.90, 51.51, 102.81, 115.01, 116.88, 117.70, 118.09, 127.69, 146.18, 147.54, 149.34, 158.05, 166.08, 170.17 ppm. (+)FABMS: m/z 585 (MH$^+$). Anal. Calcd (found) for $C_{27}H_{32}N_6O_9 \cdot 0.5HCl \cdot 1MeOH \cdot 3H_2O$: C, 47.56 (47.89); H, 6.06 (6.02); N, 11.88 (11.81).

Yield of [Fe^{III}(**6**)]$^-$ (red solid): 85%. Mp: >300 °C. (−)ESMS: m/z 636.1 ([M + 2H]$^-$). Anal. Calcd (found) for $C_{27}H_{28}FeKN_6O_9 \cdot 2HCl \cdot 0.5H_2O \cdot MeOH$: C, 39.00 (39.01); H, 4.09 (3.99); N, 9.75 (9.59). UV−vis: $\lambda = 526$ nm ($\epsilon = 3500$ M^{-1} cm^{-1}), 413 nm ($\epsilon = 5000$ M^{-1} cm^{-1}). IR: ν 1637 m, 1551 s, 1529 s, 1457 m, 1294 m, 1240 s, 1225 s, 1159 w, 743 m, 717 m cm^{-1}.

Fluorescence Quenching Binding Assay. Fluorescence quenching of recombinant Scn was measured on either a Jobin Yvon fluoroLOG-3 fluorimeter or a Cary Eclipse fluorescence spectrophotometer. A 5 nm slit band-pass for excitation and a 10 nm slit band-pass for emission were used with a high-voltage detector. An excitation wavelength of $\lambda_{exc} = 281$ nm was used, and emission was collected at $\lambda_{em} = 340$ nm. Measurements were made at a protein concentration of 100 nM in buffered aqueous solutions, plus 32 μg/mL ubiquitin (Sigma) and 5% DMSO. Fluorescence values were corrected for dilution upon addition of substrate. Fluorescence data were analyzed by nonlinear regression analysis of fluorescence response versus substrate concentration using a one-site binding model as implemented in DYNAFIT.[29] All standard binding experiments were done at pH 7.4 using TBS aqueous buffer. Control experiments were performed to ensure the stability of the protein at experimental conditions, including the dilution and the addition of DMSO and ubiquitin.

Substrate Solutions Preparation. Metal complex solutions were freshly prepared *in situ*. An aliquot of a DMSO stock solution of the free ligand (4 mM, 25 μL) and metal salt (1 equiv) were combined, vigorously shaken, and diluted with TBS buffer to form the metal complex at a concentration of 0.1 mM. The solutions were equilibrated for 1 h and diluted to a final concentration of 6 μM in 5% DMSO, aqueous buffer (pH 7.4). Apo ligand solutions were prepared analogously without the addition of a metal salt.

Structure Solution and Refinement. X-ray data sets were collected either at the Advanced Light Source ([Fe^{III}tren(CAM)$_2$(1,2-HOPO)]$^{2-}$ and [Fe^{III}tren(CAM)(1,2-HOPO)$_2$]$^-$) or on a SMART diffractometer ([Fe^{III}tren(1,2-HOPO)$_3$]^0). The data sets were collected, solved, and refined as previously described.[41−45] Structural overlays were calculated in MERCURY.[22]

[Fe^{III}tren(CAM)$_2$(1,2-HOPO)]$^{2-}$. Crystals of ferric tren-(CAM)$_2$(1,2-HOPO) were grown from a solution of complex in DMF diffused with a mixture of diethyl ether and DMF. The complex crystallized as pink plates. Two potassium counterions, a DMF molecule, and four waters (three of which were disordered) were found in the asymmetric unit.

[Fe^{III}tren(CAM)(1,2-HOPO)$_2$]$^-$. Crystals of ferric tren(CAM)(1,2-HOPO)$_2$ were grown from a solution of complex in DMF diffused with a mixture of diethyl ether and DMF. The complex crystallized as blue rhombohedral plates. A potassium counterion and two disordered DMF molecules were found in the asymmetric unit.

[Fe^{III}tren(1,2-HOPO)$_3$]^0. Crystals of ferric tren(1,2-HOPO)$_3$ were grow from a saturated solution of complex in dichloromethane by evaporation. The complex crystallized as bluish plates. Two disordered dichloromethane molecules were found in the asymmetric unit.

Computational Methods. Computational studies were conducted at the Molecular Graphics and Computation Facility, College of Chemistry, University of California, Berkeley. To determine the quadrupole moments, Θ_{zz}, the aromatic structures were geometry optimized and characterized via frequency calculations at the RHF/6-311G** level of theory in the Gaussian 03[31] package. To determine the aromatic−cation interaction energies, the aromatic structures, the sodium cation, and the aromatic−cation complexes were characterized via a frequency calculation at the MP2/6-311++G** level of theory and the aromatic−cation interaction energies corrected for basis set superposition error with the counterpoise method in the Gaussian 03[31] package. In the aromatic−cation calculations, the sodium ion was fixed at a distance of 2.47 Å above the centroid of the aromatic unit.

Supporting Information Available: Three X-ray crystallographic files in CIF format; crystallographic data table and a fluorescence binding figure; complete ref 31. This material is available free of charge via the Internet at http://pubs.acs.org.

JA8074665

(41) Szigethy, G.; Xu, J.; Gorden, A. E. V.; Teat, S. J.; Shuh, D. K.; Raymond, K. N. *Eur. J. Inorg. Chem.* **2008**, 2143−2147.
(42) *SHELXTL* (V.5.10), Crystal Structure Determination Package; Bruker Analytical X-ray Systems, Inc.: Madison, WI, 1997.
(43) *XPREP* (V.6.12), part of SHELXTL Crystal Structure Determination Package; Bruker Analytical X-ray Systems, Inc.: Madison, WI, 2001.
(44) *SAINT*, SAX Area-Detector Integration Program, V.6.40; Bruker Analytical X-ray Systems, Inc.: Madison, WI, 2003.
(45) *SADABS*, Bruker Nonius Area Detector Scaling and Absorption V.2.05; Bruker Analytical X-ray Systems, Inc.: Madison, WI, 2003.